








Research article

Evaluation of the use of carbon nanotubes recovered from a biodegradation process in the production of new biodegradable polymer nanocomposites

Ana Paula Bernardo da Silva¹, Cássia Costa Giroto¹, Thaís Larissa Amaral Montanheiro^{1,2},
Marcelo Alexandre de Farias³, Larissa Stieven Montagna¹, Dayane Batista Tada⁴,
Fernando Henrique Cristovan⁵, Ana Paula Lemes^{1*}

¹Laboratory of Polymer and Biopolymer Technology (TecPBio), Universidade Federal de São Paulo, Talim, 330, São José dos Campos, 12231-280 São Paulo, Brazil

²Laboratory of Nanotechnology, Division of Fundamental Sciences, Instituto Tecnológico de Aeronáutica, Praça Marechal Eduardo Gomes, 50, São José dos Campos, 12228-900 São Paulo, Brazil

³Brazilian Nanotechnology National Laboratory (LNNano), Brazilian Center for Research in Energy and Materials (CNPEM), Campinas, 113083-970 São Paulo, Brazil

⁴Nanomaterials and Nanotoxicology Laboratory, Universidade Federal de São Paulo, Talim, 330, São José dos Campos, 12231-280 São Paulo, Brazil

⁵Universidade Federal de Jataí, Instituto de Ciência Exatas e Tecnologia, Câmpus Jatobá, BR 364, km 195, 3800, 75801-615 Jataí, GO, Brazil

Received 13 July 2022; accepted in revised form 23 September 2022

Abstract. The present study carried out the characterization of carbon nanotubes (CNT) recovered from the biodegradation process of poly(3-hydroxybutyrate-co-3-hydroxyvalerate) (PHBV)/CNT nanocomposites and the use of this recovered CNT (CNT-rec) in the production of new PHBV nanocomposites. The results obtained by characterization of CNT-rec were very similar to the CNT. Therefore, it was possible to state that CNT properties were preserved during the biodegradation process; however, CNT-rec contained impurities such as proteins and residual PHBV. Regarding the performance as nanofillers, although both CNT and CNT-rec decreased the thermal stability of nanocomposites compared to neat PHBV, this effect was less intense in the CNT-rec nanocomposites. It is expected that both nanofillers acted as nucleating agents in the PHBV matrix crystallization process but with different effectiveness. There was no significant difference between the electrical conductivity comparing PHBV/CNT 2% and PHBV/CNT-rec 2% nanocomposites. Therefore, the recovery and use of CNT-rec is a feasible process.

Keywords: nanocomposites, biodegradable polymers, carbon nanotubes recovered, poly(3-hydroxybutyrate-co-3-hydroxyvalerate), biopolymers

1. Introduction

The search for environmentally friendly materials has motivated a lot of investigations in academia and industry. In this regard, biodegradable polymers have stood out as an alternative material mainly to replace synthetic polymers and in the production of materials

from renewable resources [1, 2]. However, with the advancement in the production and use of biodegradable polymers, new questions have arisen in the literature. The effective biodegradation of these materials when disposed of in a conducive environment. The possibility of recycling increases their useful life

*Corresponding author, e-mail: aplemess@gmail.com

© BME-PT

in the market since many have a higher production cost than conventional materials. And whether contaminants are generated during the biodegradation process since many of them are processed with other materials and additives.

Therefore, studying the biodegradation of both biodegradable polymers from renewable and synthetic sources is extremely important [3, 4]. These studies have proven that these polymers are indeed biodegraded, but there is still a lack of information regarding methods that allow ensuring the complete biodegradation of the majority of the biopolymers and that they are suitable for disposal in certain biodegradation media [5]. Siracusa [6] pointed out the difficulty of ensuring that all synthetic biodegradable polymers are suitable for composting, noting the possible contamination of the environment by polymer fragments. The author also highlighted the importance of having the polymer entirely biodegraded. Other polymers already in commercial use (in plastic bags) and reported as 100% biodegradable did not show the same results in biodegradation studies performed in the laboratory and at home-composting conditions. The polymers did not suffer total decomposition, mainly at home-composting conditions, thus alerting them to the unbridled use of this material that is reported as suitable for biodegradation [7].

In this context, the concerns regarding the waste of biodegradable polymers have to be the same raised by the waste of petroleum-based thermoplastic polymers. Considering the current limitations of the biodegradation process and the higher production cost in comparison with those derived from petroleum, recycling biopolymers has emerged as a prominent research field. Despite being still little explored, recycling biopolymers has been proven to be economically, ecologically, and technologically advantageous. Some biodegradable polymers may present more viable recycling steps than petroleum-based polymers, making their use even more attractive [8]. However, it is noted that recycling is more beneficial for biodegradable polymers with thickness above 1 mm, and when the polymer is thinner, it is more profitable to recover it (proper collection) before it is disposed of by composting rather than recycling because thinner polymers degrade more easily [8, 9]. Although numerous works that reported on recovery by recycling, biodegradation test, or even toxicity (such as ecotoxicity with plants) of biodegradable polymers are observed [1, 4, 10–12], the composites

or nanocomposites produced with these polymers have been very little considered [13, 14]. Commonly, biodegradable polymers are processed with other polymers (polymer blends) or reinforced with filler or nanofiller, generating composites or nanocomposites with enhanced properties [2, 15–25]. Few studies address the effect of the addition of the nanofiller on the polymer biodegradation property [4, 21, 26–32], and even fewer studies have investigated what happens to the nanofillers after polymer biodegradation [26]. Since most parts of the inserted nanofillers are not biodegradable, studies about their destination should be considered in the research of nanocomposites. Just as important, strategies for reusing these nanocomposites or a part of them, such as the nanoparticles themselves, should also be considered.

Among the biodegradable polymers produced from renewable resources and synthesized from microbial fermentation is the family of polyhydroxyalkanoates (PHAs). Poly(3-hydroxybutyrate-co-3-hydroxyvalerate) (PHBV) is one of the copolymers of this family with great prominence in the production of composites and nanocomposites [33–40]. Some of our previous studies have focused on the analysis of the effect of the introduction of filler and nanofiller on the biodegradation of PHBV. Titanium dioxide (TiO₂) nanoparticles or glassy carbon (GC) were shown to not affect the biodegradation of PHBV nanocomposites [31, 41]. Nevertheless, the introduction of CNT or graphite nanosheets (GNS) decreased the biodegradation rate with increasing nanofiller content [26, 30, 42, 43]. The lower biodegradation rate was associated with changes caused on the material surface, hydrophilicity, and exposure of the nanofiller to the biodegradable material. Added to this, in our previous study [26], it was observed that with the biodegradation of the nanocomposite films, the CNTs were exposed and released into the reaction medium as part of the biodegradation residues. PHBV/CNT 2% nanocomposite films were biodegraded in a liquid medium on a large scale for 20 was analyzed by field emission scanning electron microscope. It was observed that CNT was intact after the test, reinforcing the importance of an adequate treatment of the waste and indicating the possibility of recovery of these CNT after the biodegradation process.

CNT used as reinforcement in biodegradable polymeric matrices has been largely reported in the scientific literature [17, 22, 44–51]. However, the characterization and reuse of the CNT after the process

of biodegradation of these matrices have not been investigated yet. Due to the chemical and structural properties of CNT, it is expected that these properties will be unchanged in the biodegradation process, encouraging their recovery for reuse in the same material or in the production of other nanocomposites and products. This process would close the life cycle of this material and meet the principles of sustainability in the development of products. Thus, the present study carried out the characterization of CNT recovered in a biodegradation process of PHBV/CNT nanocomposites to evaluate the preservation of their properties and consequently provide crucial information to evaluate their reuse. Furthermore, the recovered CNT was used in the production of PHBV nanocomposites. The as-prepared PHBV nanocomposites with recovered CNT (PHBV/CNT-rec) were characterized regarding thermal, morphological, and electrical properties. The comparison with the properties of PHBV nanocomposite prepared with CNT and CNT-rec pointed out the successful recovery process of CNT and the use of these CNT to obtain nanocomposites with similar properties.

2. Experimental

2.1. Materials

Multiwalled carbon nanotubes (CNT) were supplied by CNT CO. Ltd. (Incheon, Korea). The CNT were produced by chemical vapor deposition with a purity of 93% (weight), diameter in the range of 10 to 40 nm, and length in the range of 5 to 20 μm . Poly(3-hydroxybutyrate-co-3-hydroxyvalerate) was supplied by PHB Industrial Ltd. (São Paulo, Brazil), with 15 mol% of hydroxyvalerate units and average molecular weight (M_w) of 230.000 $\text{g}\cdot\text{mol}^{-1}$. To prepare the films, chloroform (CHCl_3) from LabSynth (Diadema, Brazil) was used as a solvent.

2.2. Nanocomposites films preparation

Films of PHBV/CNT nanocomposites were prepared by solution-casting according to the methodology determined in previous works [25, 26, 52, 53]. PHBV was solubilized in chloroform under heating, with 8% (w/v). A suspension of CNT in chloroform was previously sonicated in an ultrasonic processor (VCX 750 Sonics, 750 W; 20 kHz) for 2 min. The solution and suspension, PHBV and CNT in chloroform, were sonicated for 1 min and then poured onto Petri plates. The films were formed after the evaporation of the chloroform overnight. PHBV nanocomposite films

were produced with 0, 1, and 2 wt% CNT and labeled as PHBV, PHBV/CNT 1%, and PHBV/CNT 2%.

2.3. CNT recovery

The CNT recovered (CNT-rec) were obtained from the biodegradation of films from the PHBV/CNT 2% nanocomposites following the methodology developed by our research group and previously reported [26]. The films were incubated in a mineral solution with a microorganisms consortium previously extracted from the soil at 32 $^{\circ}\text{C}$ with the agitation of 130 rpm for 20 days until complete biodegradation of the polymer. The CNT released in the solution was recovered in a centrifugation process and later washed again (four times). After each centrifugation step, the supernatant was discarded, and a volume of deionized water was added to the suspension with the CNT-rec. Aliquots containing the final mass of CNT-rec with deionized water were frozen and then lyophilized at -84°C for 24 h in a Labconco Free Zone 2.5 Plus Lyophilizer (Missouri, USA). CNT-rec was used to produce new films, following the same methodology of preparation of the nanocomposites (Section 2.2). Nanocomposites films were produced with 1, and 2 wt% CNT-rec labeled as PHBV/CNT-rec 1% and PHBV/CNT-rec 2%.

2.4. Characterization of CNT

Pristine CNT and CNT-rec were analyzed in a field emission gun scanning electron microscope (FEG-SEM) model MIRA 3 (TESCAN, Brno, Czech Republic) operating at 20 kV. A transmission electron microscope (TEM) JEOL JEM 1400Plus (JEOL, Japan) was used to obtain images of the pristine CNT and CNT-rec, operating at 80 kV. The nanofillers were placed on carbon-coated copper grids.

Fourier transform infrared (FT-IR) spectroscopy was performed using a Shimadzu IR Affinity-1 (Kyoto, Japan), with 2 cm^{-1} resolution, to confirm the presence of impurities remaining or molecules adhering to the CNT-rec surface. Pristine CNT and CNT-rec were prepared onto potassium bromide (KBr) crystals. Pristine CNT and CNT-rec were analyzed by Raman Renishaw 2000 spectrometer (Renishaw, Old Town, Gloucestershire, UK), coupled to an optical microscope with an argon laser (514 nm).

The samples were submitted to X-ray diffraction in a high-resolution X-ray diffractometer Philips X-Pert MRD (Eindhoven, Netherlands), with $K_{\alpha 1}$ (1542 \AA) of a copper tube operating under 45 kV and 40 mA.

The data were collected over a range of scattering angles (2θ) of 10–40°, time per step of 20 s, and step size of 0.02°.

2.5. Characterization of nanocomposites films

Differential scanning calorimeter (DSC) measurements of PHBV/CNT and PHBV/CNT-rec nanocomposites were performed using a Netzsch model DSC 204 Phoenix (Selb, Germany). Samples were sealed in an aluminum DSC pan and heated from room temperature to 200 °C at 10 °C·min⁻¹, and they were kept at this temperature for 2 min. Posteriorly, samples were cooled to -20 °C at 10 °C·min⁻¹, held at this temperature for 1 min, and again heated to 200 °C at 10 °C·min⁻¹. Measurements were performed under a nitrogen atmosphere with a flow rate of 50 ml·min⁻¹. The degree of crystallinity, X_c [%], was calculated according to Equation (1):

$$X_c [\%] = \frac{\Delta H_m}{\phi_{\text{PHBV}} \cdot \Delta H_m^0} \cdot 100 \quad (1)$$

where ΔH_m is the total melting enthalpy on second heating, ϕ_{PHBV} is the weight fraction of PHBV in the nanocomposite, and ΔH_m^0 is the theoretical melting-heat value of 100% crystalline PHBV, which was taken as 109 J·g⁻¹ [54]. ϕ_{PHBV} was considered equal to 0.99 and 0.98 for nanocomposites with 1 and 2 wt% nanofiller, respectively.

Thermogravimetric analyses (TGA) of PHBV/CNT and PHBV/CNT-rec nanocomposites were performed using Netzsch TG 209 F1 Iris[®] equipment (Selb, Germany). Samples were heated at a rate of 20 °C·min⁻¹, starting from 50 to 800 °C, under nitrogen flow.

DC conductivity of the nanocomposites was measured using the two probe method and equipment of Keithley 2400 SourceMeter (Keithley Instruments, Inc., Cleveland, OH, USA). The films had an average thickness of 40 μm, and the electrical contact was gold/palladium thin film deposited by a Sputter Coater SCD 050 Baltec (Scotia, NY, USA) on both sides of the sample producing a metal–nanocomposite–metal structure. The values were calculated using Equation (2):

$$\sigma = \frac{iL}{VA} \quad (2)$$

where σ is the electrical conductivity [S·cm⁻¹]; i is the electric current [A]; L is the sample thickness [cm]; V is the voltage [V], and A is the electrical contact area [cm²].

The cryogenically fractured surfaces of nanocomposite films were analyzed by FEG-SEM in TESCAN (model MIRA 3) equipment (Brno, Czech Republic). The samples were fractured in liquid nitrogen, fixed in aluminum stubs with carbon tape, and covered with a thin layer of gold deposited by a Sputter Coater SCD 050 BalTec (Scotia, NY, USA).

3. Results and discussion

3.1. Characterization of CNT

3.1.1. Morphology: FEG-SEM and TEM

FEG-SEM analyzes were performed to evaluate CNT morphology and possible changes resulting from the biodegradation process. The long length (Figure 1a), homogeneity in diameter size, and surface integrity of the nanotubes (Figure 1b) can be observed in the micrographs of the pristine CNT.

In the same way, in Figure 1c, it is possible to observe the presence of CNT-rec in large quantities in the residual recovered after the biodegradation test. However, the residual still presents some regions of CNT-rec with the PHBV matrix that had not been fully degraded in the biodegradation process (indicated in Figure 1c with arrows). In our previous work, Silva *et al.* [26] also showed the great presence of CNT in the final residue of the biodegradation of PHBV/CNT 2% films, and in some regions, the presence of the PHBV matrix that has not been fully degraded. An area with several CNT-rec with part of its length completely free from the matrix can be observed in Figure 1c, whereas in Figure 1d, regions of its length adhere to the polymer matrix (indicated by arrows). In Figure 1d, free CNT-rec with diameters similar to those of pristine CNTs (in the 30 nm range) can be observed, indicating that despite the biodegradation process, the structure of the CNT is preserved. In this micrograph, one can also notice the presence of CNT-rec with parts completely inserted inside the matrix, as indicated by the white arrows. The morphology of CNT-rec due to the biodegradation process was further investigated by TEM. Figure 2a–2c shows the TEM micrographs of the original CNT, where it is possible to see CNT with different lengths and diameters and the presence of amorphous carbon (Figure 2a). These structures are already expected since they are known to be formed during thermochemical vapor deposition (TCVD). It is also noted black spherical particles that correspond to the metallic catalyst particles, which are the main impurity arising from the process of obtaining

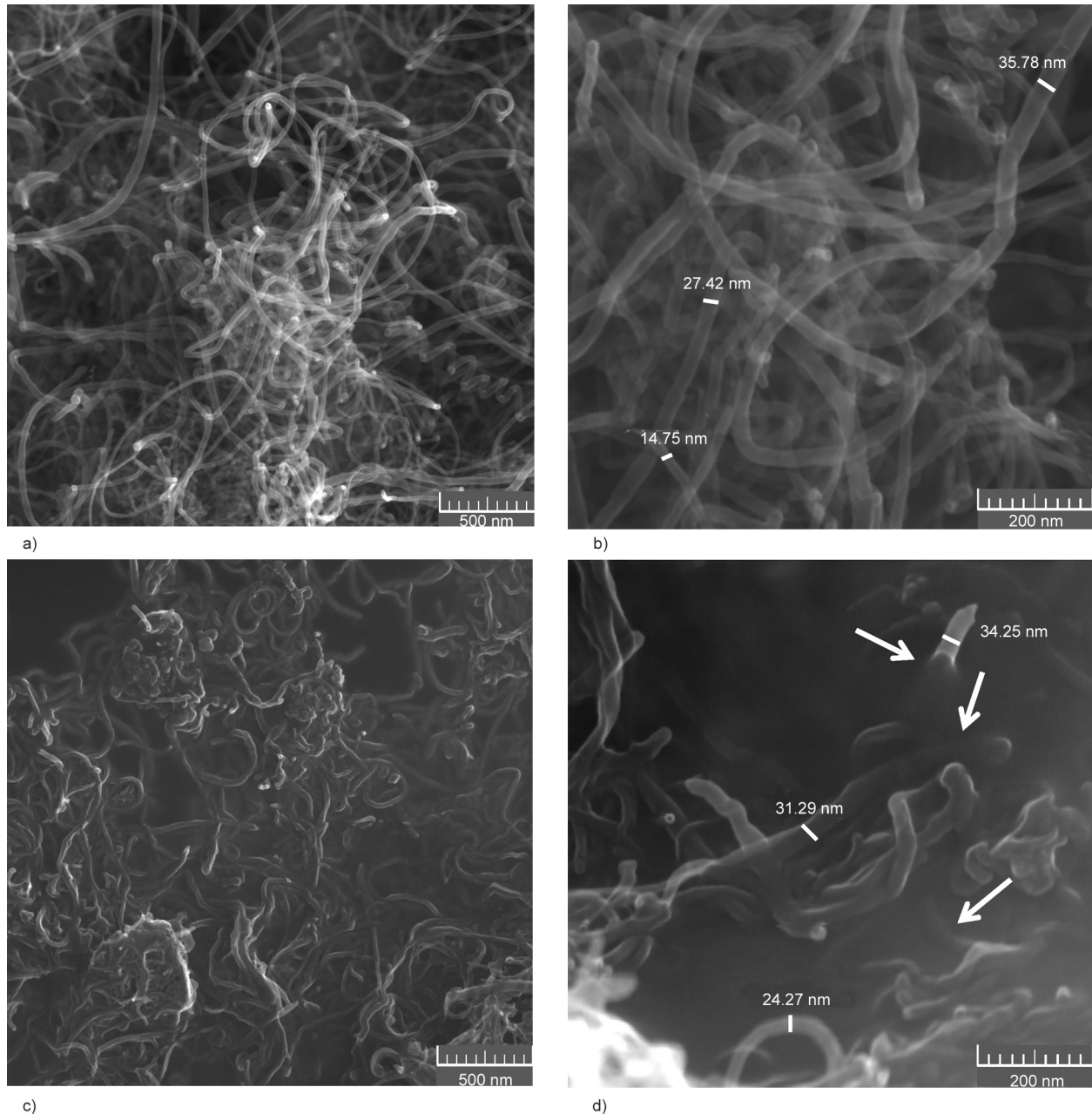


Figure 1. FEG-SEM images of (a, b) pristine CNT; (c, d) CNT-rec.

the CNT. CNT agglomerates can also be observed (indicated by arrows in [Figure 2b](#)). The presence of CNT agglomerate (darker region), amorphous carbon, and metallic catalyst particles have already been identified in our previous work [25]. In addition, the micrograph with the highest magnification ([Figure 2c](#)) shows some conical closed ends (indicated by the arrows) that are typical of not oxidized CNT, and it is believed that the formation occurs due to the presence of pentagonal rings inserted between the hexagonal rings that make up the graphite sheet [55].

In the micrographs, it is possible to notice the presence of residues from the biodegradation process around the CNT-rec (indicated in [Figure 2d](#) with

arrows), probably the non-biodegraded PHBV and residue from the biodegradation test, confirming what was observed in the SEM micrographs ([Figure 1](#)). Two factors may have caused the non-biodegradation of the PHBV still present in the CNT-rec: A possible antimicrobial activity of the CNT [56–59], which hindered the biodegradation process of the PHBV chains that were physically attached to the CNTs; The period of time in which the test was performed (20 days), which may not have been enough to complete the action of the microorganisms.

In the analysis of the CNT-rec, black spherical particles are noted, which are also observed in the pristine CNT, where they refer to the presence of the

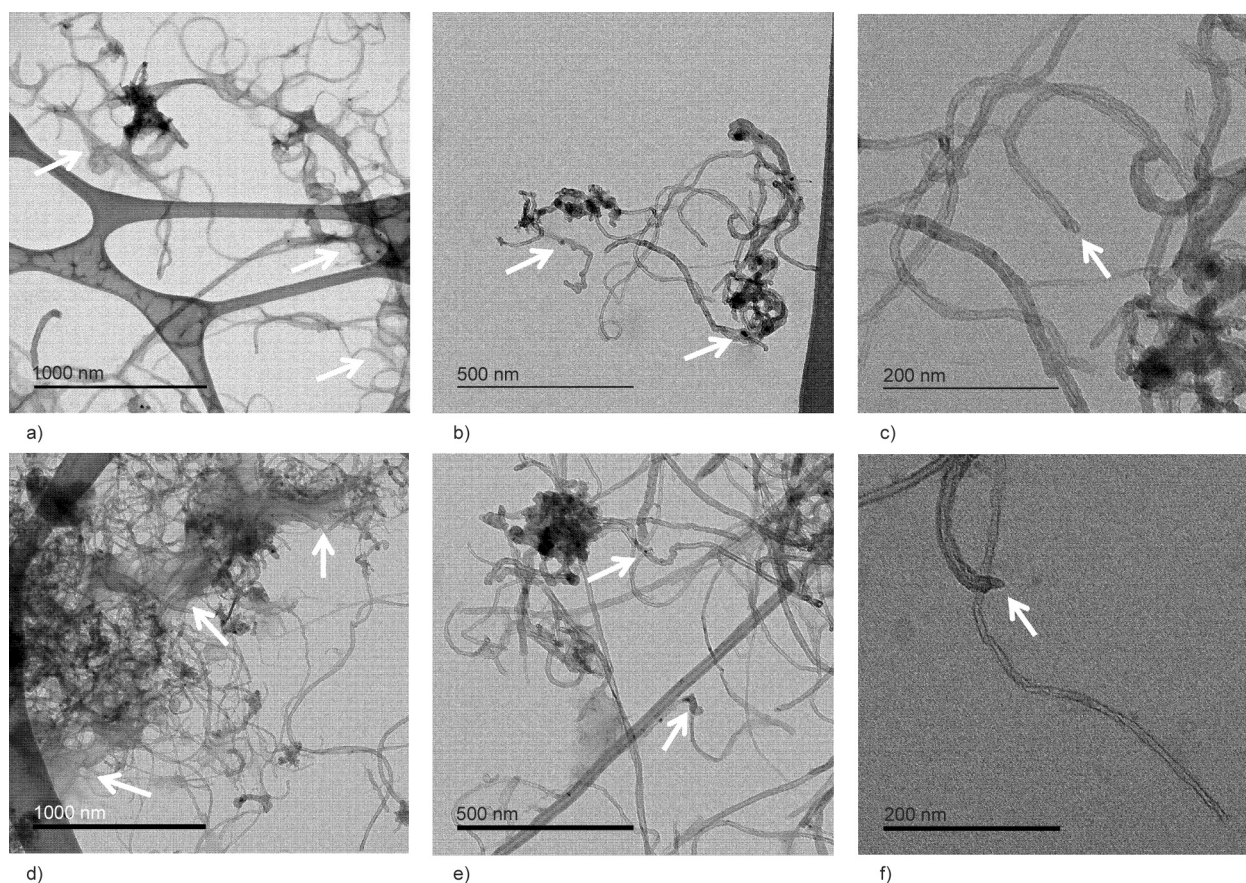


Figure 2. TEM images of (a–c) pristine CNT and (d–f) CNT-rec.

metallic catalyst particles used in the CNT production method (Figure 2e). The arrow (Figure 2f) indicates that the tip of the CNT-rec is closed; that is, it has not been oxidized in the biodegradation process, indicating that the structure of the CNT-rec has not been damaged.

3.1.2. FT-IR spectroscopy

Figure 3 shows spectra of PHBV, CNT-rec, and pristine CNT. In the PHBV spectra, the characteristic bands of this neat polymer are verified, which are present in other works in the literature [33, 60, 61]. FT-IR was used to characterize structural changes in the CNT-rec from the biodegradation process compared to the pristine CNT.

In the spectrum of CNT-rec, the broad band at 3450 cm^{-1} is more intense compared with pristine CNT. This band is assigned to the OH stretching of carboxylic groups ($\text{O}=\text{C}-\text{OH}$), and is related to the water molecules that the impurities present in the CNT-rec may have absorbed during storage [62]. Spectrum bands at 2926 and 2870 cm^{-1} , observed in pristine CNT and CNT-rec, are assigned to the asymmetric and symmetric stretching of the methylene present in the hexagonal structure of CNT. The

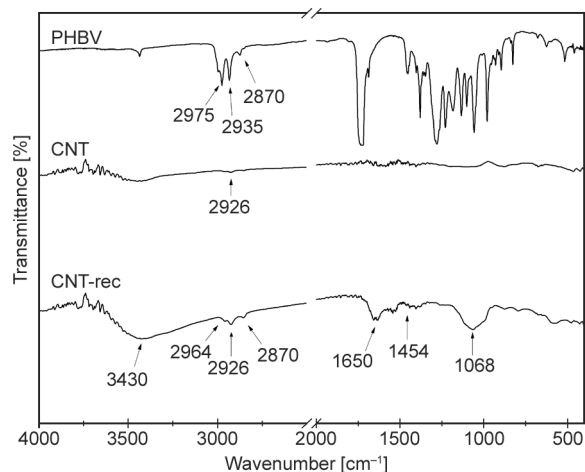


Figure 3. FT-IR spectra of the neat PHBV, pristine CNT, and CNT-rec.

identification of these bands in the CNT is related to defects in the sidewalls of the nanotubes [63]. In the spectrum of CNT-rec, some bands from the remaining PHBV are observed, indicating the presence of PHBV chains in this CNT after the biodegradation process. In addition, another band characteristic of PHBV is observed in the CNT-rec at 1454 cm^{-1} that is assigned to asymmetric angular deformation of methyl groups in the polymeric chain of PHBV [12,

33, 60]. The remaining bands of PHBV in the spectrum of CNT-rec are in accordance with the results from FEG-SEM and TEM, confirming the presence of small amounts of non-degraded PHBV.

The FT-IR spectrum of CNT-rec also shows the bands at 1650 and 1068 cm^{-1} that are characteristic of the amide functional group I and can be assigned to the presence of proteins since proteins have intense transmittance bands at those wavenumbers. The band at 1650 cm^{-1} refers to C=O stretching vibration with a small participation of the C–C–N deformation, out-of-phase C–N stretching vibration, and NH in-plane bend. And the band at 1068 cm^{-1} refers to NH_2 deformation vibration [64, 65]. These bands are additional indications of the presence of protein adhered to the surface of the CNT-rec, being a remnant of the biodegradation process. These proteins are expected to be produced by the microorganisms and released into the reaction medium. Therefore, as observed in the morphological characterizations, the existence of impurities adhered to the CNT-rec is noted (as observed in TEM images, Figure 2), which in this case indicates that the PHBV did not biodegrade completely, remaining attached to the CNT-rec, and also the residues of the biodegradation process, which in this case, maybe protein molecules.

3.1.3. Raman spectroscopy

Information about the degree of disorder of the crystal structure can be obtained through Raman spectroscopy, an analysis widely used to characterize carbon materials [66]. All graphitic materials, including CNT, exhibit a strong peak at 1580 cm^{-1} (G band), which is the first-order mode attributed to symmetry vibrations, known as E_{2g} , associated with perfect graphite [67–70]. Since most carbonaceous materials exhibit significant disorders, other bands are observed. A band near 1350 cm^{-1} called the defect band (D1 band) is attributed to the A_{1g} symmetry vibration mode of the graphite lattice, being caused by structural defects and the presence of heteroatoms. The band at 1620 cm^{-1} (D2 band) is assigned to lattice vibration analogous to the G band, but this

vibration is from the graphene layers that are not sandwiched between two graphene layers. The band near 1530 cm^{-1} (D3 band) is assigned to the amorphous sp^2 -bonded carbon species, and this band is presented in poorly ordered materials, organic molecules, fragments, or functional groups. The band at 1150 cm^{-1} (D4 band) is assigned to sp^3 - sp^2 mixed sites at the edges of crystallites or C–C and C=C stretching vibrations of polyene-like structures [68–70]. Figure 4 presents Raman spectra (experimental curve), their respective deconvolutions (fit peak curve), and the cumulative peak curve for pristine CNT and CNT-rec. The methodology used for deconvolutions is described by Sadezky *et al.* [68]. The combination of bands generated an R -square greater than 0.99, being close to 1, which characterizes an adequate fit (the theoretical curves and the values were obtained using OriginPro 8.5 software.). The bands discussed (G, D1, D2, D3, and D4) are detected in both samples, pristine CNT and CNT-rec.

To determine the degree of disorder in the structure of CNT, the ratio between the relative intensities of the D1 and G bands (ID_1/IG) is usually calculated, which is presented in Table 1. The ID_1/IG ratio tends to be higher for materials with higher defect density. For the analyzed samples, the ID_1/IG ratios are 1.25 for pristine CNT and 1.03 for CNT-rec, which suggests that CNT-rec has fewer defects in its structure compared with pristine CNT. However, since the

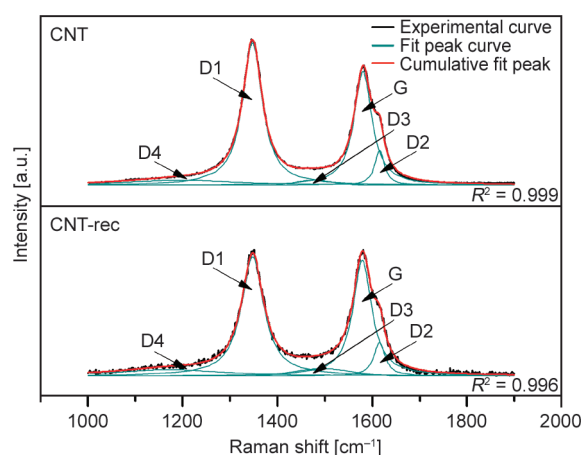


Figure 4. Raman spectra and deconvolution for pristine CNT and CNT-rec.

Table 1. Raman parameters calculated for pristine CNT and CNT-rec.

Sample	Intensity			Area ratio				
	D1	G	ID1/IG	D1/All	D2/All	D3/All	D4/All	G/All
CNT	0.98	0.78	1.25	0.49	0.06	0.02	0.08	0.35
CNT-rec	0.82	0.79	1.03	0.44	0.06	0.05	0.09	0.36

presence of mineral salts is observed in the XRD results of CNT-rec, this impurity can have caused the change in the D1 band intensity of CNT-rec (Table 1). Therefore, the ratios between the areas of each band and the total area (sum of all areas) are calculated to correlate the organization of this CNT structure and possible defects or impurities (Table 1). Thus, it can be seen that the other bands that are also attributed to defects and impurities (D2, D3, and D4) do not have a significant decrease between CNT-rec and pristine CNT; on the contrary, the ratio between D3/all-area and D4/all area have an increase. This result indicates that in the case of the D3/all area ratio of the CNT-rec (which is higher when compared to the ratio of pristine CNT), there is a great number of defects and/or impurities that can be attributed to the presence of organic molecules, fragments or functional groups [68, 69], and the presence of minerals [71]. Bar-Ziv *et al.* [71] relate the band's appearance around 1500 cm^{-1} to the presence of mineral matter observed in mineral-rich coal samples. The increase in the D3/all area ratio indicates the presence of $\text{sp}^3\text{-sp}^2$ bonds or C–C and C=C stretching vibrations characteristic of polyene-like structures [68, 69] and the presence of ionic impurities [68]. This result can indicate the presence of parts of the PHBV chain in the CNT-rec. Cuesta *et al.* [72] attribute the presence of this band to impurities and thus would not be linked to the degree of disorder of the material, which in this case is not a disorder of graphite. That being so, in the Raman analysis, as in the previous analyses, the presence of mineral salts and PHBV as impurities in the CNT-rec are also observed, but it is also observed that the biodegradation process does not affect the CNT structure of the CNT-rec, thus enabling its recovery after this process.

3.1.4. X-ray diffraction (XRD)

CNT X-ray diffractograms are characteristic of crystalline solids, which provide information regarding structural changes and/or the presence of impurities. Figure 5 shows the diffractograms of the pristine CNT and CNT-rec. As can be seen, both curves show peaks at approximately $2\theta = 26.1^\circ$, which is characteristic of graphitic structure on the walls of the carbon nanotubes, reflection from the 002 planes of graphite [73, 74]. However, the intensity of this peak in the CNT-rec curve is lower when compared with that observed for the pristine CNT. This can indicate that CNT-rec still has residues from the PHBV

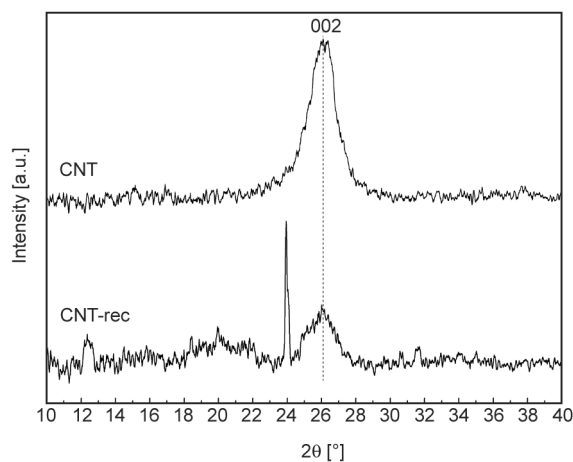


Figure 5. XRD diffractometer curves of CNT and CNT-rec.

matrix and the biodegradation process, as observed in morphological analyses (Figure 1 and Figure 2) and results of FT-IR.

CNT-rec diffractogram presents an unexpected peak at $2\theta = 24^\circ$, which can be associated with possible residues from the biodegradation test, such as mineral salts. This peak is characteristic of potassium dihydrogen phosphate (KH_2PO_4) [75, 76], one of the mineral salts used in the biodegradation test [26]. Even with the washings by centrifugation, some remnant of this salt remained in the CNT-rec or in the PHBV mass, which is observed in the micrographs, and thus detected in the XRD.

The presence of PHBV can also be noted in the X-ray diffractogram of CNT-rec, where small elevations in the curve can be observed exactly in the characteristic regions of the PHBV planes, which are: $2\theta = 13^\circ$ referring to the 020 plane, a slight elevation between $19\text{--}23^\circ$ where it contains the 021, 101, and 11 planes, and a slight displacement, shoulder, at 26° that may be due to the 121 plane at $2\theta = 25^\circ$. All these planes are presented and discussed in our previous work [17]. These plans are characteristic of the orthorhombic structure of PHBV [16, 53, 77]. Since PHBV appears as an impurity in CNT-rec, these peaks do not appear as evident as when observed in an XRD of its nanocomposite, but comparing CNT-rec to pristine CNT may indicate the presence of PHBV.

3.2. Characterization of nanocomposites films

3.2.1. Differential scanning calorimeter (DSC)

DSC analyses are performed to determine the crystallization and melting behaviors of PHBV and its nanocomposites with CNT and CNT-rec. Figure 6

shows the DSC curves for the cooling (after the first heating to eliminate the thermal history) and the second heating of the PHBV, PHBV/CNT, and PHBV/CNT-rec nanocomposites. The values of crystallization temperature (T_c) obtained in the cooling and the melting temperature (T_m), melting enthalpy (ΔH_m), and degree of crystallinity (X_c) obtained in the second heating of PHBV and nanocomposites can be observed in Table 2.

In the cooling curves (Figure 6a and Figure 6c), it can be seen that for pure PHBV, the crystallization peak occurs at a lower temperature than nanocomposites with CNT and CNT-rec. This result suggests that both the pristine CNT and the CNT-rec acted as nucleating agents, providing the previous crystallization of the PHBV matrix. The effect of the CNT nucleating agent on the PHBV matrix is also observed in the DSC results of the PHBV/CNT films with the addition of 1 to 10% CNT [25, 52, 54]. When well dispersed, CNTs increase the number of nucleation sites and, consequently, increase the polymer crystallization rate [54,

78]. In the case of CNT-rec (T_c at $\sim 75^\circ\text{C}$), this effect is less pronounced than the pristine CNT (T_c at $90\text{--}98^\circ\text{C}$), probably due to the lower actual concentration of CNT-rec. The characterizations of the CNT (Section 3.1) reveal that the CNT-rec contained impurities from the biodegradation process; therefore, the actual concentration of CNT in the PHBV/CNT-rec may be lower than the added mass of CNT in the PHBV/CNT nanocomposites.

In the curves of the second heating of pure PHBV (Figure 6b and Figure 6d), a melting peak of 170°C and a small shoulder in the curve of 157°C are observed. For the PHBV/CNT and PHBV/CNT-rec nanocomposites, it is possible to observe two melting peaks related to different lamella sizes of the crystalline phase, related to the homogeneous and heterogeneous PHBV nucleation [39, 79]. The introduction of CNT and CNT-rec intensifies this bimodal distribution due to its influence on the nucleation of the crystals that can occur both in heterogeneous and homogeneous nucleation, as already observed for the

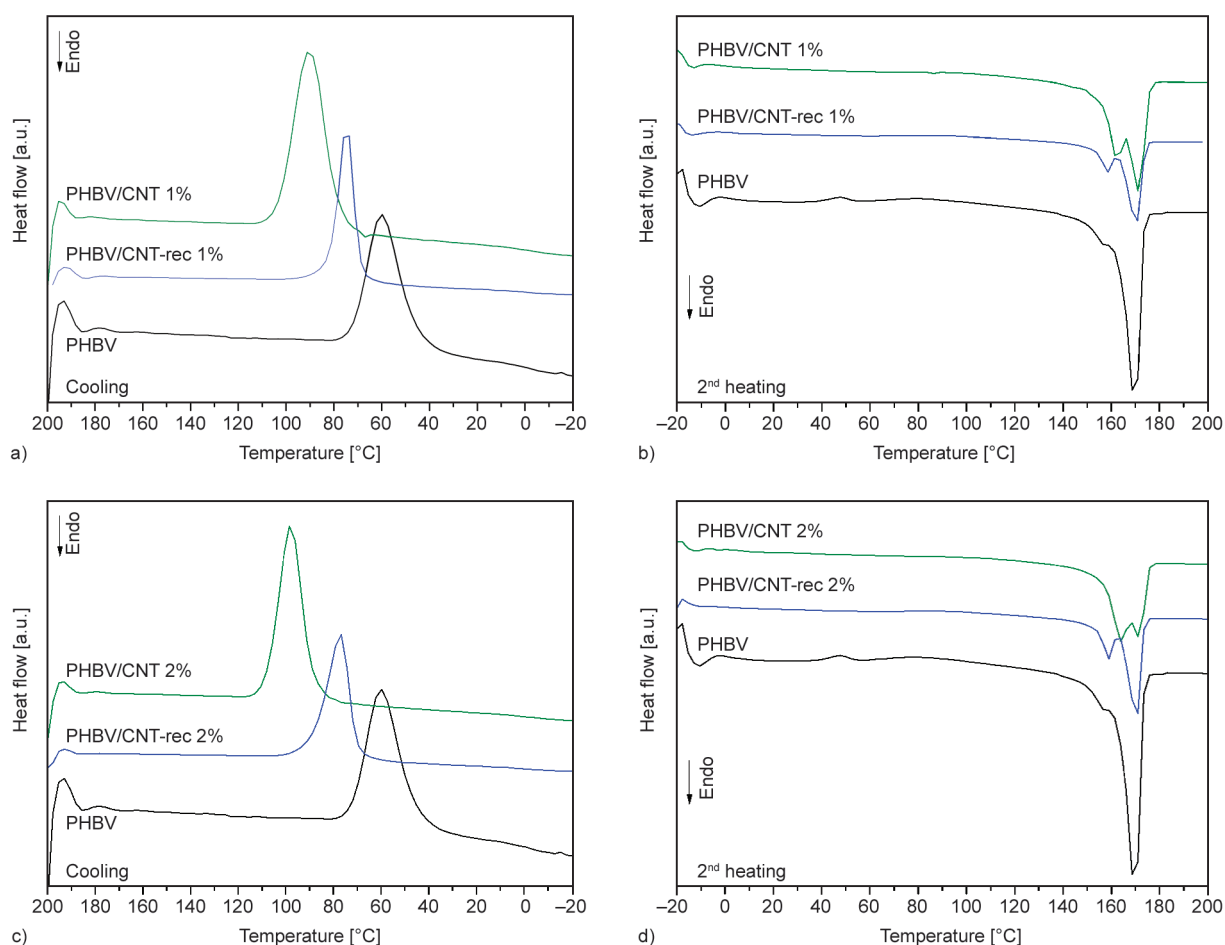


Figure 6. DSC curves of neat PHBV, PHBV/CNT 1%, and PHBV/CNT-rec 1%: (a) cooling and (b) second heating. Neat PHBV, PHBV/CNT 2% and PHBV/CNT-rec 2%: (c) cooling and (d) second heating.

introduction of CNT and other nanoparticles in the PHBV matrix [16, 39, 41, 54, 80]. Still, for the CNT-rec nanocomposite, this first peak appears with lower intensity when compared to the CNT pristine nanocomposite, which again indicates a lower actual nanofiller concentration in these films. The variations in the melting temperatures (T_{m1} and T_{m2}) are not significant when comparing all samples.

Table 2 also shows a decrease in the degree of crystallinity with the addition and increase of CNT concentration. Although CNT acts as a nucleating agent, when homogeneously dispersed in polymeric matrices and higher concentrations, they can act as a physical barrier, due to their length, for the growth of crystallites, hindering the crystallization of the polymer [17, 81]. The PHBV/CNT nanocomposite has a higher degree of crystallinity than PHBV/CNT-rec, which may be related to the better distribution of CNT in the matrix and the more real content of CNT in the final material. The most significant decrease in the degree of crystallinity (~40%) in PHBV/CNT-rec nanocomposites compared to pure PHBV may be related to impurities from the biodegradation process, as proven in other analyzes (morphology, FT-IR, Raman, and XRD). The contaminants, such as salts and protein, present in CNT-rec act as a barrier to the diffusion and folding of polymeric chains in the crystalline phase during crystallization. In this way, the PHBV matrix crystallization process is hampered since the mobility of the chains is restricted, and the PHBV/CNT-rec nanocomposites show a lower degree of crystallinity [36]. Furthermore, in the case of PHBV/CNT-rec nanocomposites, no significant difference is observed between the different concentrations, as in the case of PHBV/CNT nanocomposites, probably because the 2% mass of CNT-rec does not correspond solely to CNT, but also impurities.

Table 2. Thermal parameters evaluated from DSC for PHBV, nanocomposites PHBV/CNT and nanocomposites PHBV/CNT-rec.

Sample	T_c [°C]	T_{m1} [°C]	T_{m2} [°C]	ΔH_m [J/g]	X_c [%]
PHBV	60	N/D	170	87.07	79.9
PHBV/CNT 1%	90	163	171	72.71	67.4
PHBV/CNT-rec 1%	75	158	170	40.64	37.7
PHBV/CNT 2%	98	164	172	55.16	51.6
PHBV/CNT-rec 2%	77	159	171	42.47	39.8

N/D = not determined

3.2.2. Thermogravimetric analysis (TGA)

Thermogravimetric analysis (TGA) determined the thermal degradation behavior of neat PHBV and its nanocomposites with CNT and CNT-rec in an inert atmosphere (N_2) (Figure 7). In the TGA curves of all samples (Figure 7a and Figure 7b), it is found that the thermal degradation occurred in a single step, related to the thermal degradation of the PHBV matrix, which is proven by the curves of the first derivative (DTG) (Figure 7c and Figure 7d). The thermal degradation of the PHBV occurs by transesterification and cis-elimination [82]. To determine the effect of the introduction of the CNT and CNT-rec in the thermal degradation of the PHBV matrix, the temperature at 1% weight loss ($T_{1\%}$), the onset temperature (T_{onset}), the temperature at the maximum weight loss (T_{max}), and the residual mass (RM) are shown in Table 3.

In the $T_{1\%}$, an increase in the thermal stability in all nanocomposites is observed after the introduction of CNT. The increase in $T_{1\%}$ is more evident for nanocomposites with 1 and 2% of pristine CNT. This increase can be related to the decrease in the transport of combustion gas during the polymer decomposition with the addition of CNT and causing the absorption of free radicals produced in the degradation of the carbon surface [83]. A similar result is also reported in our previous work [52] in PHBV/MWCNT and PHBV/functionalized MWCNT nanocomposites and by Lai *et al.* [83] with the addition of MWCNT in PHBV nanocomposites.

However, the onset degradation temperature (Table 3) does not show the same trend. The T_{onset} of PHBV/CNT 1%, PHBV/CNT-rec 1%, and PHBV/CNT-rec 2% nanocomposites are almost the same as PHBV. But a small decrease of 7 °C in the T_{onset} of PHBV/CNT 2% nanocomposite is observed. The difficulty of CNT dispersion can have caused this effect on this concentration in the PHBV matrix. In the production of PHBV/MWCNT nanocomposites, Lemes *et al.* [25] observed that the increase of MWCNT concentration does not improve the thermal stability in the same proportion, and they attribute this result to the difficulty of nanofiller dispersion. Although, in other words, the increase in the thermal stability is observed in PHBV nanocomposites with 0.5 wt% of MWCNT, where the nanofiller act as a barrier to the permeation of combustion gas in nanocomposites with good dispersion of the MWCNT [52].

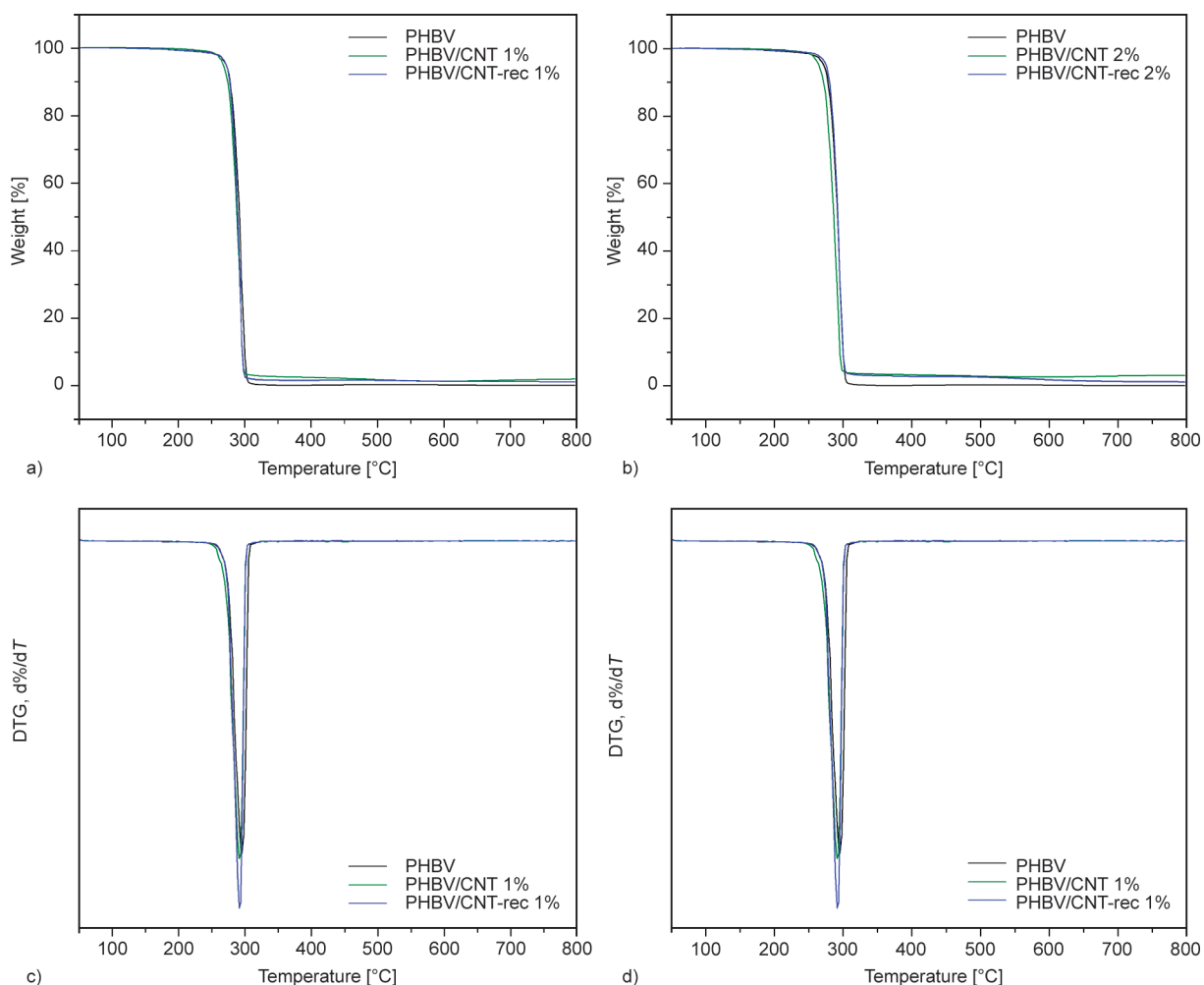


Figure 7. Thermogravimetric curves of PHBV, nanocomposites PHBV/CNT and nanocomposites PHBV/CNT-rec. a) and b) thermogravimetric curves; c) and d) first derivative curves.

Comparing the two nanocomposites with the content of 2%, PHBV/CNT 2%, and PHBV/CNT-rec 2%, the same behavior of decreased thermal stability is not observed. PHBV/CNT-rec 2% may have maintained the same temperature range as PHBV due to the actual content of CNT inserted being smaller in this nanocomposite since, as previously observed, CNT-rec contained not only CNT but also impurities. Thus, in the case of PHBV/CNT-rec nanocomposites, the

Table 3. Temperature at 1% weight loss ($T_{1\%}$), onset temperature (T_{onset}), temperature of maximum weight-loss rate (T_{max}), and residual mass (RM) for PHBV, PHBV/CNT, and PHBV/CNT-rec nanocomposites.

Sample	$T_{1\%}$ [°C]	T_{onset} [°C]	T_{max} [°C]	RM [%]
PHBV	225	282	303	0,02
PHBV/CNT 1%	245	280	297	1,97
PHBV/CNT-rec 1%	230	280	297	1,08
PHBV/CNT 2%	242	275	299	3,11
PHBV/CNT-rec 2%	240	283	302	1,16

non-variation of thermal stability may be related to the presence of impurities from the biodegradation process, such as the polymer itself.

In the T_{max} results (Table 3), the addition of 1% CNT causes a small decrease of 6 °C in the temperature value for the nanocomposites with pristine CNT and CNT-rec and of 4 °C for the PHBV/CNT 2%. This small decrease can be associated with CNT dispersion in the polymer; since not being well dispersed, the nanofiller does not act as a transport barrier for combustion gases, as was expected [83]. With the addition of 2% CNT-rec, no significant variation is observed compared to PHBV, which may also be associated with nanofiller dispersion in the matrix. In addition, the presence of PHBV in the CNT-rec may have collaborated in not affecting more expressively (impairing) the thermal stability of the nanocomposite. Lai *et al.* [83] observe an increase of 16 °C in T_{max} for PHBV nanocomposites with 2% of MWCNT and relate this increase to the

effective dispersion of the MWCNT, that act as a barrier to thermal degradation of the polymer.

As expected, the *RM* value obtained for the PHBV films is very close to 0% since, at this temperature, it is expected that the entire polymer has already degraded. The *RM* of nanocomposite with 1 and 2% pristine CNT show values well above the expected value, close to the added CNT content for each nanocomposite, since this is supposed to be the residue from the thermal degradation of the nanocomposites. However, this value is proportional for both nanocomposites. In the previous work of this research group [52], it was also observed an increase in *RM* value compared to the content of CNT in PHBV/MWCNT nanocomposites, being justified by the more active surface of the pristine CNT, which prevented the degradation of a small part of the polymer. Meanwhile, for the PHBV/CNT-rec 1% and PHBV/CNT-rec 2% nanocomposites, lower *RM* values are noticed compared to the content of CNT in the PHBV/CNT-rec nanocomposites. The difference in the *RM* value of the PHBV/CNT-rec 2% is even greater. This effect may be associated with the real content of CNT-rec that was added being lower since the CNT-rec still contained impurities arising from the biodegradation process as observed in the characterization of CNT-rec and which may have suffered thermal degradation.

Results obtained from the TGA analysis show that even with impurities in the CNT-rec, the PHBV/CNT-rec nanocomposites present suitable thermal stability, and under some conditions, it is even better than the thermal stability obtained by the addition of pristine CNT. These results further support our claim that the recovery and reuse of these carbon materials after the biodegradation process of the films is a feasible strategy.

3.2.3. Morphology

Cryogenically fracture surfaces of PHBV/CNT, and PHBV/CNT-rec nanocomposites were analyzed by FEG-SEM micrographs (Figure 8). The PHBV/CNT 1% (Figure 8a) shows a smooth fracture surface typical of a brittle and hard material; in addition, it is possible to observe the presence of CNT in the PHBV matrix (white arrows). On the other hand, PHBV/CNT-rec 1% (Figure 8c) presents a slightly rougher surface, characteristic of a material that suffered some deformation before rupture. But in this region of the micrograph, it is impossible to observe

the presence of CNTs, only possible impurities (white arrows), which may be linked to a smaller amount of nanofiller than the added content and the nanofiller not being well dispersed in the polymer matrix, due to the agglomerates.

PHBV/CNT 2% (Figure 8b) presents a rougher surface than other nanocomposites, indicating that it suffered a greater deformation before rupture. In comparison with the PHBV/CNT 1% nanocomposite, the increase in the content of CNT may also have contributed to the increase in roughness. CNT is present in the PHBV matrix (white arrows) with good interaction between nanofiller and polymer. However, in other works with this same CNT content, it is possible to observe the presence of a greater amount of CNT well dispersed in the polymer [83] or to identify the nanofiller's poor dispersion in large areas agglomerates [25]. Therefore, the micrograph of PHBV/CNT 2% (Figure 8b) may indicate the heterogeneity of the nanocomposite and thus may not represent regions that may contain the CNT poorly dispersed in the polymer matrix. This would be in agreement with the results observed in TGA, that the poor dispersion impaired the improvement of the thermal degradation temperatures of the nanocomposites.

A single CNT (white arrow) is observed on the fracture surface of PHBV/CNT-rec 2% (Figure 8d), in addition to a smooth surface, characteristic of a brittle and hard material, and the presence of impurities (white circles). Similar to the PHBV/CNT-rec 1% nanocomposite, this result indicates that the amount of CNT in the nanocomposite is lower. This is also in agreement with the other characterizations that stated the non-real content (being 2% in this nanocomposite) of the CNT and the presence of impurities (white circles).

3.2.4. Electrical conductivity

Electrical conductivity measurements are performed to verify the influence of the addition of CNT (pristine CNT and CNT-rec) to the PHBV matrix and the possible consequences of the biodegradation process on the electrical properties of CNT-rec. The values were calculated using Equation (2) through the linear portion of the *I-V* curves obtained from the equipment and are shown in Table 4. The PHBV shows the behavior of an insulating polymer, as observed by the electrical conductivity value ($5.1 \cdot 10^{-13} \text{ S} \cdot \text{cm}^{-1}$) [52]. The addition of CNT can turn the nanocomposite

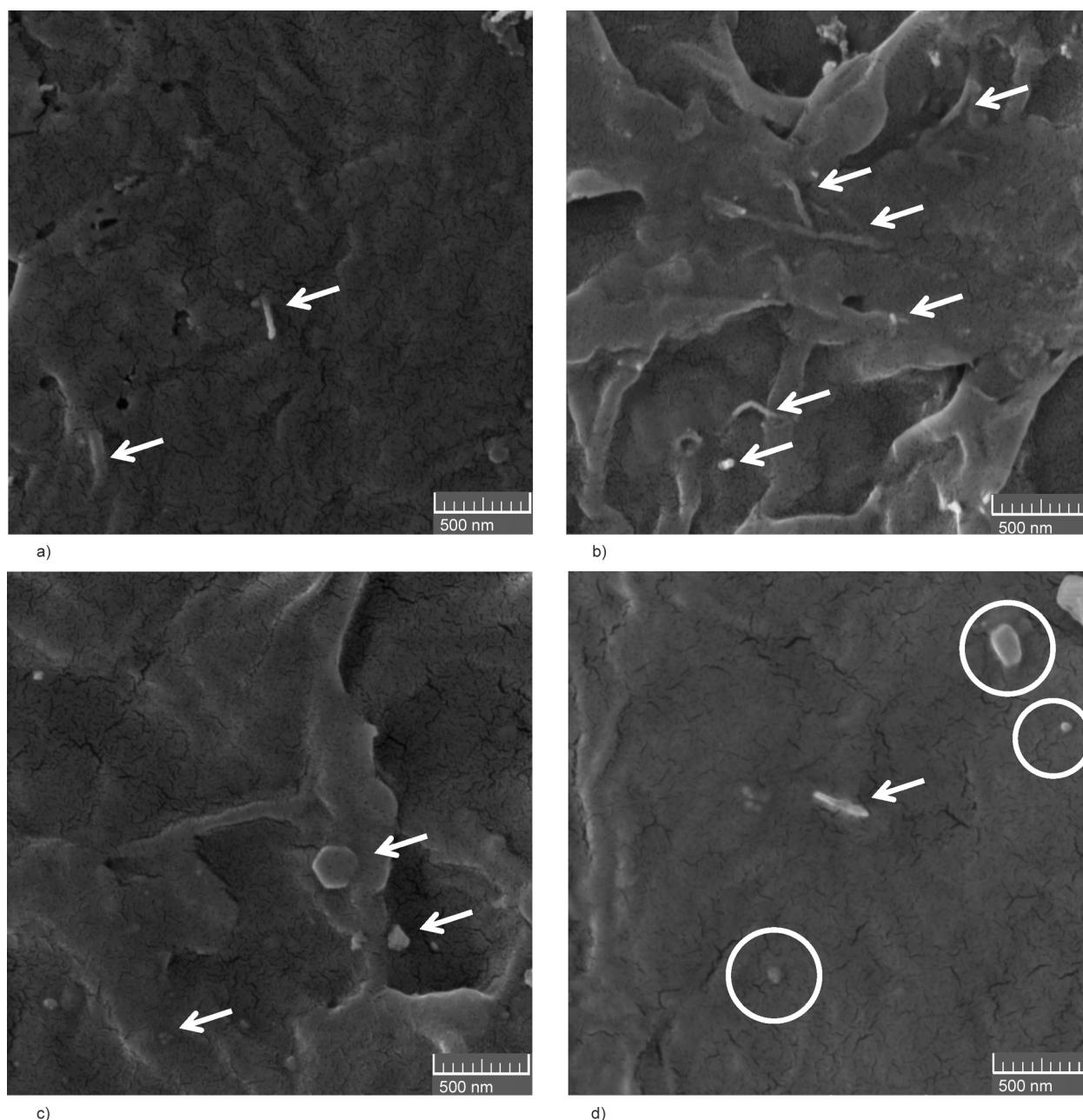


Figure 8. FEG-SEM micrographs of (a) PHBV/CNT 1%, (b) PHBV/CNT 2%, (c) PHBV/CNT-rec 1%, and, (d) PHBV/CNT-rec 2% nanocomposites.

into a semiconductor or conductive material up to a certain value (percolation threshold). The percentage

Table 4. Electrical conductivity values of PHBV, nanocomposites PHBV/CNT, and nanocomposites PHBV/CNT-rec.

Sample	Conductivity [S·cm ⁻¹]
PHBV*	$5.10 \cdot 10^{-13}$
PHBV/CNT 1%	$5.77 \cdot 10^{-4}$
PHBV/CNT-rec 1%	$4.18 \cdot 10^{-11}$
PHBV/CNT 2%	$1.42 \cdot 10^{-2}$
PHBV/CNT-rec 2%	$1.41 \cdot 10^{-2}$

*Value of the reference [52]

of CNT greatly influences the electrical conductivity of the nanocomposite, so this property tends to increase according to the increase in the percentage of the nanofiller [84, 85].

As expected, the addition of 1% CNT to the PHBV provides a significant improvement in the electrical conductivity of the nanocomposite, an increase of 9 orders of magnitude, when compared to the values of pure PHBV. The improvement in the electrical property supposes that a conductive network of CNT is formed in the polymeric matrix, thus allowing the transport of electrons in the nanocomposite [85]. The electrical conductivity of PHBV/CNT-rec 1%

nanocomposite ($4.18 \cdot 10^{-11} \text{ S} \cdot \text{cm}^{-1}$) is lower by 7 orders of magnitude compared to PHBV/CNT 1% ($5.77 \cdot 10^{-4} \text{ S} \cdot \text{cm}^{-1}$) and an increase of 2 orders of magnitude compared of pure PHBV. This result can be justified due to the amount of residual PHBV and impurities present in the CNT-rec, making the actual mass of CNT-rec in nanocomposite less than that mentioned, as already discussed and presented in other analyses.

Within this context, it would be expected that the electrical conductivity in the case of PHBV/CNT-rec 2% nanocomposite would also be lower compared to that of PHBV/CNT 2% nanocomposite due to the lower real concentration of CNT-rec. Surprisingly, there is no significant difference between the electrical conductivity of the PHBV/CNT 2% nanocomposite ($1.42 \cdot 10^{-2} \text{ S} \cdot \text{cm}^{-1}$) and the PHBV/CNT-rec 2% ($1.41 \cdot 10^{-2} \text{ S} \cdot \text{cm}^{-1}$). This result indicates that even with a concentration of less than 2% CNT, this amount can be sufficient to reach the percolation threshold in the PHBV/CNT-rec 2% film and thus result in a conductivity value close to the film with 2% CNT. The increase compared to pure PHBV is 11 orders of magnitude for both PHBV/CNT-rec 2% and PHBV/CNT 2%.

Therefore, electrical conductivity measurements of PHBV nanocomposite reveal that the biodegradation process does not compromise the electrical properties of CNT-rec, which corroborates with the results of previous analyses that observed the integrity of CNT-rec after the biodegradation process. Therefore, it is possible to state that it is possible to obtain nanocomposites with the same electrical properties when using pristine CNT or CNT-rec.

4. Conclusions

The use of carbon nanotubes recovered (CNT-rec) from the biodegradation of PHBV/CNT nanocomposites films to produce new nanocomposites with PHBV matrix is viable and very promising. Since the life cycle of this material can be closed in a relatively short period, it is full of sustainable principles of new material development. The methodology applied in this work shows that it is possible to recover the CNT from the biodegradation of PHBV/CNT nanocomposites; however, the CNT-rec still contained impurities such as proteins, mineral salts, and the PHBV matrix that were not fully biodegraded, thus indicating that the CNT recovery process needs to be improved. Despite that, it is found that CNT-rec

maintains its main structural characteristics. Comparing the properties of PHBV/CNT and PHBV/CNT-rec nanocomposites, it is noted that the effect of these nanofillers on the matrix is very close, mainly concerning the thermal and electrical properties of the nanocomposites. In some cases, despite observing the same trend, the changes of the PHBV properties are less evident in the PHBV/CNT-rec, probably due to the lower accurate content of CNT-rec in the nanocomposite since the nanofiller contains impurities arising from the biodegradation process. Regarding electrical conductivity, which can be considered a key property of the final application of the nanocomposite, there is no significant difference between the PHBV/CNT and PHBV/CNT-rec nanocomposites. Therefore, the results reported herein show that the recovery of the CNT from a nanocomposite is a feasible process that results in CNT with similar properties to the original ones and that the CNT recovered can be applied to produce new samples of the PHBV nanocomposite also with similar properties of the original nanocomposite.

Acknowledgements

The authors would like to thank the Instituto Nacional de Pesquisas Espaciais (INPE) for Raman measurements, DRX analyses, and SEM-FEG images and the Centro Nacional de Pesquisa em Energia e Materiais (CNPEM) for TEM images. The authors are grateful to João Paulo Barros Machado for the help in the Raman measurements and DRX analyses.

This work was supported by the Coordenação de Aperfeiçoamento de Pessoal de Nível Superior (CAPES) – Finance Code-001. The authors acknowledge the financial support received from Fundação de Amparo à Pesquisa do Estado de São Paulo (FAPESP 2019/15976-0 and 2017/24873-4) and Conselho Nacional de Desenvolvimento Científico e Tecnológico (CNPq 313989/2018-4).

References

- [1] Zhong Y., Godwin P., Jin Y., Xiao H.: Biodegradable polymers and green-based antimicrobial packaging materials: A mini-review. *Advanced Industrial and Engineering Polymer Research*, **3**, 27–35 (2020).
<https://doi.org/10.1016/j.aiepr.2019.11.002>
- [2] Armentano I., Puglia D., Luzi F., Arciola C. R., Morena F., Martino S., Torre L.: Nanocomposites based on biodegradable polymers. *Materials*, **11**, 795 (2018).
<https://doi.org/10.3390/ma11050795>
- [3] Kliem S., Kreutzbruck M., Bonten C.: Review on the biological degradation of polymers in various environments. *Materials*, **13**, 4586 (2020).
<https://doi.org/10.3390/ma13204586>

- [4] Meereboer K. W., Misra M., Mohanty A. K.: Review of recent advances in the biodegradability of polyhydroxyalkanoate (PHA) bioplastics and their composites. *Green Chemistry*, **22**, 5519–5558 (2020).
<https://doi.org/10.1039/d0gc01647k>
- [5] Lamparelli R. C. B. C., Montagna L. S., da Silva A. P. B., do Amaral Montanheiro T. L., Lemes A. P.: Study of the biodegradation of PLA/PBAT films after biodegradation tests in soil and the aqueous medium. *Biointerface Research in Applied Chemistry*, **12**, 833–846 (2022).
<https://doi.org/10.33263/BRIAC121.833846>
- [6] Siracusa V.: Microbial degradation of synthetic biopolymers waste. *Polymers*, **11**, 1066 (2019).
<https://doi.org/10.3390/polym11061066>
- [7] Adamcová D., Zloch J., Brtnický M., Vaverková M. D.: Biodegradation/disintegration of selected range of polymers: Impact on the compost quality. *Journal of Polymers and the Environment*, **27**, 892–899 (2019).
<https://doi.org/10.1007/s10924-019-01393-3>
- [8] Stachowiak T., Łukasik K.: The management of polymer and biodegradable composite waste in relation to petroleum-based thermoplastic polymer waste – In terms of energy consumption and processability. *Sustainability*, **13**, 3701 (2021).
<https://doi.org/10.3390/su13073701>
- [9] Scaffaro R., Maio A., Sutera F., Gulino E. F., Morreale M.: Degradation and recycling of films based on biodegradable polymers: A short review. *Polymers*, **11**, 651 (2019).
<https://doi.org/10.3390/polym11040651>
- [10] Weng Y-X., Wang X-L., Wang Y-Z.: Biodegradation behavior of PHAs with different chemical structures under controlled composting conditions. *Polymer Testing*, **30**, 372–380 (2011).
<https://doi.org/10.1016/j.polymertesting.2011.02.001>
- [11] Alshehrei F.: Biodegradation of synthetic and natural plastic by microorganisms. *Journal of Applied & Environmental Microbiology*, **5**, 8–19 (2017).
<https://doi.org/10.12691/jaem-5-1-2>
- [12] Wei L., McDonald A. G.: Accelerated weathering studies on the bioplastic, poly(3-hydroxybutyrate-co-3-hydroxyvalerate). *Polymer Degradation and Stability*, **126**, 93–100 (2016).
<https://doi.org/10.1016/j.polymdegradstab.2016.01.023>
- [13] Kumar V., Sehgal R., Gupta R.: Blends and composites of polyhydroxyalkanoates (PHAs) and their applications. *European Polymer Journal*, **161**, 110824 (2021).
<https://doi.org/10.1016/j.eurpolymj.2021.110824>
- [14] Eraslan K., Aversa C., Nofar M., Barletta M., Gisario A., Salehiyan R., Goksu Y. A.: Poly(3-hydroxybutyrate-co-3-hydroxyhexanoate) (PHBH): Synthesis, properties, and applications - A review. *European Polymer Journal*, **167**, 111044 (2022).
<https://doi.org/10.1016/j.eurpolymj.2022.111044>
- [15] Lizundia E., Sarasua J. R., D'Angelo F., Orlacchio A., Martino S., Kenny J. M., Armentano I.: Biocompatible poly(L-lactide)/MWCNT nanocomposites: Morphological characterization, electrical properties, and stem cell interaction. *Macromolecular Bioscience*, **12**, 870–881 (2012).
<https://doi.org/10.1002/mabi.201200008>
- [16] Montagna L. S., do Amaral Montanheiro T. L., Machado J. P. B., Passador F. R., Lemes A. P., Rezende M. C.: Effect of graphite nanosheets on properties of poly(3-hydroxybutyrate-co-3-hydroxyvalerate). *International Journal of Polymer Science*, **2017**, 9316761 (2017).
<https://doi.org/10.1155/2017/9316761>
- [17] do Amaral Montanheiro T. L., Campos T. M. B., Montagna L. S., da Silva A. P., Ribas R. G., de Menezes B. R. C., Passador F. R., Thim G. P.: Influence of CNT pre-dispersion into PHBV/CNT nanocomposites and evaluation of morphological, mechanical and crystallographic features. *Materials Research Express*, **6**, 105375 (2019).
<https://doi.org/10.1088/2053-1591/ab42ed>
- [18] Backes E. H., Pires L. D. N., Beatrice C. A. G., Costa L. C., Passador F. R., Pessan L. A.: Fabrication of biocompatible composites of poly(lactic acid)/hydroxyapatite envisioning medical applications. *Polymer Engineering and Science*, **60**, 636–644 (2020).
<https://doi.org/10.1002/pen.25322>
- [19] da Silva T. F., Menezes F., Montagna L. S., Lemes A. P., Passador F. R.: Preparation and characterization of antistatic packaging for electronic components based on poly(lactic acid)/carbon black composites. *Journal of Applied Polymer Science*, **136**, 47273 (2019).
<https://doi.org/10.1002/app.47273>
- [20] Terzopoulou Z., Papageorgiou D. G., Papageorgiou G. Z., Bikiaris D. N.: Effect of surface functionalization of halloysite nanotubes on synthesis and thermal properties of poly(ϵ -caprolactone). *Journal of Materials Science*, **53**, 6519–6541 (2018).
<https://doi.org/10.1007/s10853-018-1993-1>
- [21] Zaidi Z., Mawad D., Crosky A.: Soil biodegradation of unidirectional polyhydroxybutyrate-co-valerate (PHBV) biocomposites toughened with polybutylene-adipate-co-terephthalate (PBAT) and epoxidized natural rubber (ENR). *Frontiers in Materials*, **6**, 275 (2019).
<https://doi.org/10.3389/fmats.2019.00275>
- [22] Verginio G. E. A., do Amaral Montanheiro T. L., Montagna L. S., Marini J., Passador F. R.: Effectiveness of the preparation of maleic anhydride grafted poly(lactic acid) by reactive processing for poly(lactic acid)/carbon nanotubes nanocomposites. *Journal of Applied Polymer Science*, **138**, 50087 (2020).
<https://doi.org/10.1002/app.50087>
- [23] de Oliveira Ferreira S. O., do Amaral Montanheiro T. L., Montagna L. S., Guerrini L. M., Lemes A. P.: Study of cellulose nanocrystals and zinc nitrate hexahydrate addition in chitosan hydrogels. *Materials Research*, **22**, e20180760 (2019).
<https://doi.org/10.1590/1980-5373-MR-2018-0760>

- [24] do Amaral Montanheiro T. L., Montagna L. S., Patrulea V., Jordan O., Borchard G., Ribas R. G., Campos T. M. B., Thim G. P., Lemes A. P.: Enhanced water uptake of PHBV scaffolds with functionalized cellulose nanocrystals. *Polymer Testing*, **79**, 106079 (2019).
<https://doi.org/10.1016/j.polymertesting.2019.106079>
- [25] Lemes A. P., do Amaral Montanheiro T. L., da Silva A. P., Durán N.: PHBV/MWCNT films: Hydrophobicity, thermal and mechanical properties as a function of MWCNT concentration. *Journal of Composites Science*, **3**, 12 (2019).
<https://doi.org/10.3390/jcs3010012>
- [26] da Silva A. P., do Amaral Montanheiro T. L., Montagna L. S., Andrade P. F., Durán, N., Lemes A. P.: Effect of carbon nanotubes on the biodegradability of poly(3-hydroxybutyrate-co-3-hydroxyvalerate) nanocomposites. *Journal of Applied Polymer Science*, **136**, 48020 (2019).
<https://doi.org/10.1002/app.48020>
- [27] da Silva A. P., Pereira M. P., Passador F. R., Montagna L. S.: PLA/coffee grounds composites: A study of photodegradation and biodegradation in soil. *Macromolecular Symposia*, **394**, 2000091 (2020).
<https://doi.org/10.1002/masy.202000091>
- [28] Goodwin D. G., Boyer I., Devahif T., Gao C., Frank B. P., Lu X., Kuwama L., Gordon T. B., Wang J., Ranville J. F., Bouwer E. J., Fairbrother D. H.: Biodegradation of carbon nanotube/polymer nanocomposites using a monoculture. *Environmental Science & Technology*, **52**, 40–51 (2018).
<https://doi.org/10.1021/acs.est.7b02062>
- [29] da Silva T. F., Menezes F., Montagna L. S., Lemes A. P., Passador F. R.: Effect of lignin as accelerator of the biodegradation process of poly(lactic acid)/lignin composites. *Materials Science & Engineering B*, **251**, 114441 (2019).
<https://doi.org/10.1016/j.mseb.2019.114441>
- [30] Montagna L. S., do Amaral Montanheiro T. L., Borges A. C., Koga-Ito C. Y., Lemes A. P., Rezende M. C.: Biodegradation of PHBV/GNS nanocomposites by *Penicillium funiculosum*. *Journal of Applied Polymer Science*, **134**, 44234 (2016).
<https://doi.org/10.1002/app.44234>
- [31] de Souza Vieira L., Montagna L. S., da Silva A. P. B., Verginio G. E. A., Passador F. R.: Effect of glassy carbon addition and photodegradation on the biodegradation in aqueous medium of poly(3-hydroxybutyrate-co-3-hydroxyvalerate)/glassy carbon green composites. *Journal of Applied Polymer Science*, **138**, 50821 (2021).
<https://doi.org/10.1002/app.50821>
- [32] Masood F., Aziz M., Haider H., Shakil O., Yasin T., Hameed A.: Biodegradation of gamma irradiated poly-3-hydroxybutyrate/sepiolite nanocomposites. *International Biodeterioration and Biodegradation*, **126**, 1–9 (2018).
<https://doi.org/10.1016/j.ibiod.2017.09.012>
- [33] Antunes A., Popelka A., Aljarod O., Hassan M. K., Kasak P., Luyt A. S.: Accelerated weathering effects on poly(3-hydroxybutyrate-co-3-hydroxyvalerate) (PHBV) and PHBV/TiO₂ nanocomposites. *Polymers*, **12**, 1743 (2020).
<https://doi.org/10.3390/polym12081743>
- [34] de Souza Vieira L., Montagna L. S., Marini J., Passador F. R.: Influence of particle size and glassy carbon content on the thermal, mechanical, and electrical properties of PHBV/glassy carbon composites. *Journal of Applied Polymer Science*, **138**, 49740 (2020).
<https://doi.org/10.1002/app.49740>
- [35] Rivera-Briso A. L., Serrano-Aroca Á.: Poly(3-hydroxybutyrate-co-3-hydroxyvalerate): Enhancement strategies for advanced applications. *Polymers*, **10**, 732 (2018).
<https://doi.org/10.3390/polym10070732>
- [36] Malmir S., Barral L., Bouza R., Esperanza M., Seoane M., Feijoo-Bandín S., Lago F.: Poly(3-hydroxybutyrate-co-3-hydroxyvalerate)/cellulose nanocrystal films: Artificial weathering, humidity absorption, water vapor transmission rate, antimicrobial activity and biocompatibility. *Cellulose*, **26**, 2333–2348 (2019).
<https://doi.org/10.1007/s10570-018-2216-2>
- [37] Arroyo J., Ryan C.: Incorporation of carbon nanofillers tunes mechanical and electrical percolation in PHBV:PLA blends. *Polymers*, **10**, 1371 (2018).
<https://doi.org/10.3390/polym10121371>
- [38] Dasan Y. K., Bhat A. H., Faiz A.: Polymer blend of PLA/PHBV based bionanocomposites reinforced with nanocrystalline cellulose for potential application as packaging material. *Carbohydrate Polymers*, **157**, 1323–1332 (2017).
<https://doi.org/10.1016/j.carbpol.2016.11.012>
- [39] Sridhar V., Lee I., Chun H. H., Park H.: Graphene reinforced biodegradable poly(3-hydroxybutyrate-co-4-hydroxybutyrate) nano-composites. *Express Polymer Letters*, **7**, 320–328 (2013).
<https://doi.org/10.3144/expresspolymlett.2013.29>
- [40] Bledzki A. K., Jaszkwicz A.: Mechanical performance of biocomposites based on PLA and PHBV reinforced with natural fibres – A comparative study to PP. *Composites Science and Technology*, **70**, 1687–1696 (2010).
<https://doi.org/10.1016/j.compscitech.2010.06.005>
- [41] Braga N. F., da Silva A. P., Arantes T. M., Lemes A. P., Cristovan F. H.: Physical–chemical properties of nanocomposites based on poly(3-hydroxybutyrate-co-3-hydroxyvalerate) and titanium dioxide nanoparticles. *Materials Research Express*, **5**, 15303–15317 (2018).
<https://doi.org/10.1088/2053-1591/aa9f7a>
- [42] Montagna L. S., Oyama I. C., Lamparelli R. C. B. C., Silva A. P., do Amaral Montanheiro T. L., Lemes A. P.: Evaluation of biodegradation in aqueous medium of poly(hydroxybutyrate-co-hydroxyvalerate)/carbon nanotubes films in respirometric system. *Journal of Renewable Materials*, **7**, 117–128 (2019).
<https://doi.org/10.32604/jrm.2019.00036>

- [43] Lemes A. P., do Amaral Montanheiro T. L., Passador F. R., Durán N.: Nanocomposites of polyhydroxyalkanoates reinforced with carbon nanotubes: Chemical and biological properties. in 'Eco-friendly polymer nanocomposites, advanced structured materials' (eds.: Thakur V., Thakur M.) Springer, New Delhi, 79–108 (2015).
https://doi.org/10.1007/978-81-322-2470-9_3
- [44] Singh N. K., Singh S. K., Dash D., Gonugunta P., Misra M., Maiti P.: CNT induced β -phase in polylactide: Unique crystallization, biodegradation, and biocompatibility. *The Journal of Physical Chemistry C*, **117**, 10163–10174 (2013).
<https://doi.org/10.1021/jp4009042>
- [45] Qiu Z., Wang H., Xu C.: Crystallization, mechanical properties, and controlled enzymatic degradation of biodegradable poly(ϵ -caprolactone)/multi-walled carbon nanotubes nanocomposites. *Journal of Nanoscience and Nanotechnology*, **11**, 7884–7893 (2011).
<https://doi.org/10.1166/jnn.2011.4714>
- [46] Yu H.-Y., Qin Z.-Y., Sun B., Yang X.-G., Yao J.-M.: Reinforcement of transparent poly(3-hydroxybutyrate-co-3-hydroxyvalerate) by incorporation of functionalized carbon nanotubes as a novel bionanocomposite for food packaging. *Composites Science and Technology*, **94**, 96–104 (2014).
<https://doi.org/10.1016/j.compscitech.2014.01.018>
- [47] Silva A. P. B., Montagna L. S., Passador F. R., Rezende M. C., Lemes A. P.: Biodegradable nanocomposites based on PLA/PHBV blend reinforced with carbon nanotubes with potential for electrical and electromagnetic applications. *Express Polymer Letters*, **15**, 987–1003 (2021).
<https://doi.org/10.3144/expresspolymlett.2021.79>
- [48] Russell R. A., Foster L. J. R., Holden P. J.: Carbon nanotube mediated miscibility of polyhydroxyalkanoate blends and chemical imaging using deuterium-labelled poly(3-hydroxyoctanoate). *European Polymer Journal*, **105**, 150–157 (2018).
<https://doi.org/10.1016/j.eurpolymj.2018.05.031>
- [49] Kim S., Zare Y., Garmabi H., Rhee K. Y.: Variations of tunneling properties in poly (lactic acid) (PLA)/poly (ethylene oxide) (PEO)/carbon nanotubes (CNT) nanocomposites during hydrolytic degradation. *Sensors and Actuators A: Physical*, **274**, 28–36 (2018).
<https://doi.org/10.1016/j.sna.2018.03.004>
- [50] Zare Y., Rhee K. Y.: Following the morphological and thermal properties of PLA/PEO blends containing carbon nanotubes (CNTs) during hydrolytic degradation. *Composites Part B: Engineering*, **175**, 107132 (2019).
<https://doi.org/10.1016/j.compositesb.2019.107132>
- [51] Zare Y., Rhee K. Y.: Expression of normal stress difference and relaxation modulus for ternary nanocomposites containing biodegradable polymers and carbon nanotubes by storage and loss modulus data. *Composites Part B: Engineering*, **158**, 162–168 (2019).
<https://doi.org/10.1016/j.compositesb.2018.09.076>
- [52] do Amaral Montanheiro T. L., Cristóvan F. H., Machado J. P. B., Tada D. B., Durán N., Lemes A. P.: Effect of MWCNT functionalization on thermal and electrical properties of PHBV/MWCNT nanocomposites. *Journal of Materials Research*, **30**, 55–65 (2014).
<https://doi.org/10.1557/jmr.2014.303>
- [53] do Amaral Montanheiro T. L., Montagna L. S., Machado J. P. B., Lemes A. P.: Covalent functionalization of MWCNT with PHBV chains: Evaluation of the functionalization and production of nanocomposites. *Polymer Composites*, **40**, 288–295 (2017).
<https://doi.org/10.1002/pc.24644>
- [54] Vidhate S., Innocentini-Mei L., D'Souza N. A.: Mechanical and electrical multifunctional poly(3-hydroxybutyrate-co-3-hydroxyvalerate)-multiwall carbon nanotube nanocomposites. *Polymer Engineering & Science*, **52**, 1367–1374 (2012).
<https://doi.org/10.1002/pen.23084>
- [55] Endo M., Takeuchi K., Kobori K., Takahashi K., Kroto H. W., Sarkar A.: Pyrolytic carbon nanotubes from vapor-grown carbon fibers. *Carbon*, **33**, 873–881 (1995).
[https://doi.org/10.1016/0008-6223\(95\)00016-7](https://doi.org/10.1016/0008-6223(95)00016-7)
- [56] Chung H., Son Y., Yoon T. K., Kim S., Kim W.: The effect of multi-walled carbon nanotubes on soil microbial activity. *Ecotoxicology and Environmental Safety*, **74**, 569–575 (2011).
<https://doi.org/10.1016/j.ecoenv.2011.01.004>
- [57] Kang S., Herzberg M., Rodrigues D. F., Elimelech M.: Antibacterial effects of carbon nanotubes: Size does matter! *Langmuir*, **24**, 6409–6413 (2008).
<https://doi.org/10.1021/la800951v>
- [58] Mocan T., Matea C. T., Pop T., Mosteanu O., Buzoianu A. D., Suciú S., Puia C., Zdrehus C., Iancu C., Mocan L.: Carbon nanotubes as anti-bacterial agents. *Cellular and Molecular Life Sciences*, **74**, 3467–3479 (2017).
<https://doi.org/10.1007/s00018-017-2532-y>
- [59] You Y., Das K., Guo H., Chang C.-W., Navas-Moreno M., Chan J. W., Verburg P., Poulson S. R., Wang X., Xing B., Yang Y.: Microbial transformation of multiwalled carbon nanotubes by *Mycobacterium vanbaalenii* PYR-1. *Environmental Science and Technology*, **51**, 2068–2076 (2017).
<https://doi.org/10.1021/acs.est.6b04523>
- [60] Antunes A., Luyt A. S., Popelka A., Mahmoud A., Aljarod O., Hassan M. K., Kasak P.: Influence of accelerated weathering on the physical and structural properties of poly(lactic-acid)/poly(3-hydroxybutyrate-co-3-hydroxyvalerate) (PLA/PHBV) blends. *Express Polymer Letters*, **15**, 687–707 (2021).
<https://doi.org/10.3144/expresspolymlett.2021.58>
- [61] Kann Y., Shurgalin M., Krishnaswamy R. K.: FTIR spectroscopy for analysis of crystallinity of poly(3-hydroxybutyrate-co-4-hydroxybutyrate) polymers and its utilization in evaluation of aging, orientation and composition. *Polymer Testing*, **40**, 218–224 (2014).
<https://doi.org/10.1016/j.polymertesting.2014.09.009>
- [62] Țucureanu V., Matei A., Avram A. M.: FTIR spectroscopy for carbon family study. *Critical Reviews in Analytical Chemistry*, **46**, 502–520 (2016).
<https://doi.org/10.1080/10408347.2016.1157013>

- [63] Scheibe B., Borowiak-Palen E., Kalenczuk R. J.: Oxidation and reduction of multiwalled carbon nanotubes - Preparation and characterization. *Materials Characterization*, **61**, 185–191 (2010).
<https://doi.org/10.1016/j.matchar.2009.11.008>
- [64] Barth A.: Infrared spectroscopy of proteins. *Biochimica et Biophysica Acta – Bioenergetics*, **1767**, 1073–1101 (2007).
<https://doi.org/10.1016/j.bbabi.2007.06.004>
- [65] Pretsch E., Buhlmann P., Affolter C.: *Structure determination of organic compounds: Tables of spectral data*. Springer, New York (2000).
- [66] Belin T., Epron F.: Characterization methods of carbon nanotubes: A review. *Materials Science and Engineering B: Solid-State Materials for Advanced Technology*, **119**, 105–118 (2005).
<https://doi.org/10.1016/j.mseb.2005.02.046>
- [67] Beyssac O., Goffé B., Petitot J-P., Froigneux E., Moreau M., Rouzaud J-N.: On the characterization of disordered and heterogeneous carbonaceous materials by Raman spectroscopy. *Spectrochimica Acta Part A: Molecular and Biomolecular Spectroscopy*, **59**, 2267–2276 (2003).
[https://doi.org/10.1016/S1386-1425\(03\)00070-2](https://doi.org/10.1016/S1386-1425(03)00070-2)
- [68] Sadezky A., Muckenhuber H., Grothe H., Niessner R., Pöschl U.: Raman microspectroscopy of soot and related carbonaceous materials: Spectral analysis and structural information. *Carbon*, **43**, 1731–1742 (2005).
<https://doi.org/10.1016/j.carbon.2005.02.018>
- [69] Sheng C.: Char structure characterised by Raman spectroscopy and its correlations with combustion reactivity. *Fuel*, **86**, 2316–2324 (2007).
<https://doi.org/10.1016/j.fuel.2007.01.029>
- [70] Tomaszewicz M., Mianowski A.: Char structure dependence on formation enthalpy of parent coal. *Fuel*, **199**, 380–393 (2017).
<https://doi.org/10.1016/j.fuel.2017.02.081>
- [71] Bar-Ziv E., Zaida A., Salatino P., Senneca O.: Diagnostics of carbon gasification by Raman microprobe spectroscopy. *Proceedings of the Combustion Institute*, **28**, 2369–2374 (2000).
[https://doi.org/10.1016/S0082-0784\(00\)80649-9](https://doi.org/10.1016/S0082-0784(00)80649-9)
- [72] Cuesta A., Dhamelincourt P., Laureyns J., Martínez-Alonso A., Tascón J. M. D.: Raman microprobe studies on carbon materials. *Carbon*, **32**, 1523–1532 (1994).
[https://doi.org/10.1016/0008-6223\(94\)90148-1](https://doi.org/10.1016/0008-6223(94)90148-1)
- [73] Wu F. Y., Cheng H. M.: Structure and thermal expansion of multi-walled carbon nanotubes before and after high temperature treatment. *Journal of Physics D: Applied Physics*, **38**, 4302–4307 (2005).
<https://doi.org/10.1088/0022-3727/38/24/006>
- [74] Peng Y., Liu H.: Effects of oxidation by hydrogen peroxide on the structures of multiwalled carbon nanotubes. *Industrial and Engineering Chemistry Research*, **45**, 6483–6488 (2006).
<https://doi.org/10.1021/ie0604627>
- [75] Jančaitienė K., Šlinkšienė R.: KH₂PO₄ crystallisation from potassium chloride and ammonium dihydrogen phosphate. *Polish Journal of Chemical Technology*, **18**, 1–8 (2016).
<https://doi.org/10.1515/pjct-2016-0001>
- [76] Vorontsov D., Filonenko S., Kanak A., Okrepka G., Khalavka Y.: Charge directed assembly of CdTe/CdS nanoparticles inside monocrystalline KH₂PO₄. *CrystrEngComm*, **19**, 6804–6810 (2017).
<https://doi.org/10.1039/c7ce01688c>
- [77] Öner M., Çöl A. A., Pochat-Bohatier C., Bechelany M.: Effect of incorporation of boron nitride nanoparticles on the oxygen barrier and thermal properties of poly(3-hydroxybutyrate-co-hydroxyvalerate). *RSC Advances*, **6**, 90973–90981 (2016).
<https://doi.org/10.1039/c6ra19198c>
- [78] do Amaral Montanheiro T. L., de Menezes B. R. C., Montagna L. S., Beatrice C. A. G., Marini J., Lemes A. P., Thim, G. P.: Non-isothermal crystallization kinetics of injection grade PHBV and PHBV/carbon nanotubes nanocomposites using isoconversional method. *Journal of Composites Science*, **4**, 52 (2020).
<https://doi.org/10.3390/jcs4020052>
- [79] Gunaratne L. M. W. K., Shanks R. A., Amarasinghe G.: Thermal history effects on crystallisation and melting of poly(3-hydroxybutyrate). *Thermochimica Acta*, **423**, 127–135 (2004).
<https://doi.org/10.1016/j.tca.2004.05.003>
- [80] Wang K., Wang Y., Zhang R., Li Q., Shen C.: Preparation and characterization of microbial biodegradable poly(3-hydroxybutyrate-co-4-hydroxybutyrate)/organoclay nanocomposites. *Polymer Composites*, **33**, 838–842 (2012).
<https://doi.org/10.1002/pc.22220>
- [81] da Silva B. C., dos Santos C. M., de Oliveira Couto C. A., Backes E. H., Passador F. R.: Evaluation of aging resistance in UHMWPE/LLDPE blend-based carbon nanotubes nanocomposites. *Macromolecular Symposia*, **383**, 1700079 (2019).
<https://doi.org/10.1002/masy.201700079>
- [82] Aoyagi Y., Yamashita K., Doi Y.: Thermal degradation of poly[(R)-3-hydroxybutyrate], poly[ε-caprolactone], and poly[(S)-lactide]. *Polymer Degradation and Stability*, **76**, 53–59 (2002).
[https://doi.org/10.1016/S0141-3910\(01\)00265-8](https://doi.org/10.1016/S0141-3910(01)00265-8)
- [83] Lai M., Li J., Yang J., Liu J., Tong X., Cheng H.: The morphology and thermal properties of multi-walled carbon nanotube and poly(hydroxybutyrate-co-hydroxyvalerate) composite. *Polymer International*, **53**, 1479–1484 (2004).
<https://doi.org/10.1002/pi.1566>
- [84] Sanchez-Garcia M. D., Lagaron J. M., Hoa S. V.: Effect of addition of carbon nanofibers and carbon nanotubes on properties of thermoplastic biopolymers. *Composites Science and Technology*, **70**, 1095–1105 (2010).
<https://doi.org/10.1016/j.compscitech.2010.02.015>
- [85] Aguilar J. O., Bautista-Quijano J. R., Avilés F.: Influence of carbon nanotube clustering on the electrical conductivity of polymer composite films. *Express Polymer Letters*, **4**, 292–299 (2010).
<https://doi.org/10.3144/expresspolymlett.2010.37>